PCCP

ROYAL SOCIETY OF CHEMISTRY

ARTICLE TYPE

Cite this: DOI: 10.1039/xxxxxxxxxx

4,4'-bis(2-benzoxazolyl)stilbene luminescent probe: assessment of aggregates formation through photophysics experiments and quantum-chemical calculations†

Antonella Battisti,[a,b] Matteo Ambrosetti,[c] Giacomo Ruggeri,[d] Chiara Cappelli[c] and Andrea Pucci[d]

Received Date
Accepted Date

DOI: 10.1039/xxxxxxxxxx

www.rsc.org/journalname

A combination of experimental and quantum mechanical investigations is applied to the study of the optical features of 4,4'-bis(2-benzoxazolyl)stilbene (BBS) dissolved in solution or in a poly(L-lactic acid) (PLA) thermoplastic matrix at different contents. The experimental analyses allow for the characterization of BBS solutions and dispersions in terms of absorption and emission features, along with the collection of some key parameters such as fluorescence quantum yield, anisotropy and lifetime, while the computational approach gives a detailed description of the photophysical behavior of BBS in the different environments. For 10^{-5} M BBS solutions, fluorescence spectra show the expected peaks at 425 and 455 nm of the un-interacting BBS molecules with a single fluorescence lifetime of 0.85 ns without revealing any aggregation phenomena, prevented by the short lifetime and fast diffusion rate of the monomer. Moreover, the calculated spectra are in excellent agreement with the experiments, thus showing the reliability of the computational approach. In time-resolved emission experiments (TRES) on more concentrated solutions (10^{-4} M) and on BBS crystals the presence of an excimer is revealed by the rising of a broad peak around 540 nm, followed by the disappearance of the two main peaks under 460 nm on a time scale of about 10 ns. Computational analysis attributes this behavior to the formation of aggregates of different geometries. BBS dispersions in PLA reveal the presence of different BBS architectures depending on fluorophore content. Even if at low concentrations BBS is mainly dispersed as monomer in the matrix, spheroid aggregates of about 800-900 nm in diameter are also present and the relevant fluorescence spectra arise from the combination of monomer and aggregate contributions. At higher concentrations, BBS starts forming crystals of peculiar helicoidal shape, with a diameter of about 2 μm, variable length up to several hundreds of μm and emission spectra similar to those of isolated BBS crystals.

Introduction

The study of the formation of fluorescent supramolecular aggregates of dye molecules is nowadays rapidly evolving in literature due to the emerging research on chromogenic materials.[1–4] This is documented by a class of compounds called "aggregachromic" (or fluorogenic) dyes, a term which is applied to colour effects arisen from chromophore dimerisation and aggregation.[2,5,6] Depending on the dye self-assembling characteristics and miscibility into dispersing media (solvents or polymer matrices), chromophores start to aggregate above a certain concentration into supramolecular assemblies, whose optical properties usually differ from the isolated monomer. It has been found that environmental sensing based on aggregachromic fluorophores is one of the most powerful methods for the detection of external solicitations with high sensitivity and selectivity thanks to the tailored design of the emitting probes.[7–9] Some fluorescent aggregachromic species have also been successfully used in solar collectors to im-

[a] NEST - Scuola Normale Superiore and Istituto Nanoscienze - CNR (CNR-NANO), Piazza San Silvestro 12, I-56127 Pisa, ITALY. E-mail: antonella.battisti@sns.it
[b] M3-Village, Consorzio Interuniversitario Nazionale per la Scienza e Tecnologia dei Materiali - INSTM, p.zza San Silvestro 12, I-56127 Pisa, ITALY
[c] Scuola Normale Superiore, Piazza dei Cavalieri 7, I-56126 Pisa, ITALY. E-mail: chiara.cappelli@sns.it
[d] Dipartimento di Chimica e Chimica Industriale, Universitá di Pisa, Via Moruzzi 13, I-56124 Pisa, ITALY. E-mail: andrea.pucci@unipi.it

† Electronic Supplementary Information (ESI) available: [details of any supplementary information available should be included here]. See DOI: 10.1039/cXCP00000x/

prove the efficiency of photovoltaic cells.[10,11] Among colorimetric fluorescent sensors, it is worth citing the fluorescent dye 4,4'-bis(2-benzoxazolyl)stilbene (BBS), a well-known stilbene derivative generally employed as optical brightener in many polymeric articles and textiles.[12,13] BBS has been discovered as an aggregachromic dye, a feature that makes it ideal for use in sensitive mechanochromic[14–16] and thermochromic[17–19] polymeric blends. Upon formation or breaking of BBS excited dimers (excimers), a significant blue-green chromogenic behavior can be observed under UV irradiation. The broad green emission band, which accompanies the formation of BBS aggregates, results favored by $C\text{-}H\cdots\pi$ and $\pi-\pi$ intermolecular interactions of BBS molecules in planar conformation.[20] The optical output has been recently monitored also by means of hue evaluation in the HSV color space of digital images recorded under UV illumination during the external solicitation, thus paving the way for cost-effective and sensitive tools to be used in the production of smart materials and devices.[21] Nevertheless, even if the basic optical properties and applications of BBS appear well reported in literature, the dye photophysics results meanly investigated so far.

Intrigued by the possibility of providing a complete study of BBS opto-electronic characteristics, we set out to combine high-resolution optical imaging techniques and quantum-mechanical calculations, the former making accessible the detection of nanostructures in soft-matter by non-ionizing visible radiation, and the latter being able to provide structural and spectroscopic properties of organic molecules and complex molecular systems. BBS photophysics have been first investigated in solution, focusing the attention on its aggregation behavior in different classes of solvents, together with computational investigations which have been used to obtain better insight into the nature of absorbing and emitting states both as a single molecule and as dimeric aggregates (possibly with the inclusion of solvent effects). Then, the formation of dye supramolecular structures has been also monitored in a semicrystalline biodegradable aliphatic polyester (poly(L-lactide) (PLA) solid blend, taking into consideration the relationship between the different aggregates architecture and emission response.

1 Experimental setup

1.1 Materials

The solvents dichloromethane (CH_2Cl_2), 2-propanol ($PrOH$), ethyl acetate ($AcOEt$), toluene, 1,2-dichlorobenzene and ethyl butanoate ($PrCOOEt$) were purchased from Sigma-Aldrich and used as received or purified by standard procedures. 4,4'-Bis(2-benzoxazolyl)-stilbene (*BBS*, 97%) and poly(L-lactic acid) (*PLA*, Mw 67,000) were supplied from Sigma-Aldrich and used as received.

1.2 Apparatus and Methods

BBS/PLA solid mixtures were prepared by solution-casting. More specifically, a 0.3 g sample of PLA was dissolved under stirring in 20 mL of a solution of BBS in $CHCl_3$ with desired fluorophore concentration; the solution was then cast on a Petri dish and slowly evaporated under chloroform-saturated atmosphere at a temperature of 20 °C. BBS-loaded polymeric films were recovered after 12 h. Spectrophotometric measurements on the BBS-loaded films were carried out on a Perkin Elmer Lambda 650 spectrophotometer, while fluorescence measurements were performed on a PerkinElmer LS55 spectrofluorometer. Temperature control was kept within ± 0.1 °C. Absorption spectra of BBS solutions were taken on a Jasco V550 UV/Vis spectrophotometer (JASCO, Easton, MD) by setting the monochromator slits to 2 nm, the scanning speed to 200 nm/min, the data resolution to 1 nm, and the time collection average on each wavelength interval to 0.25 s. The absorption spectrum of each sample was corrected for background and normalized to the measured optical density at 370 nm. Fluorescence measurements on BBS solutions were performed on a Cary Eclipse spectrofluorometer (Varian, Palo Alto, CA) by setting the excitation monochromator slits to 5 nm, the emission monochromator to 2.5 nm, the scanning speed to 120 nm/min, the data resolution to 1 nm, and the time collection average on each wavelength interval to 0.5 s. Excitation wavelength was set to 360 nm. ~~The fluorescence spectrum of each sample was corrected for background.~~ Fluorescence quantum yield ϕ_f was calculated according to the comparative method of Williams *et al.*,[22] taking into account the refraction index of the solvents. Fluorescein and quinine sulphate were chosen as standard fluorophores, assuming 0.92[23] and 0.54[24] respectively as quantum yield values for the standards. Fluorescence lifetime imaging (FLIM) measurements of BBS solutions and crystals were performed using a Leica TCS SP5 inverted confocal microscope (Leica Microsystems AG, Wetzlar, Germany) equipped with an external pulsed diode laser for excitation at 405 nm and a TCSPC acquisition card (PicoHarp 300, Picoquant) connected to internal spectral detectors. Laser repetition rate was set to 40 MHz. Image size was 64×64 pixels and scan speed was usually set to 400 Hz (lines per second). The pinhole aperture was set to 1.0 Airy. Solutions were placed into glass bottom cuvettes and imaged using a 63.0× 1.20 numerical aperture water immersion objective (Leica Microsystems). Polymeric films were viewed with a 100.0× 1.3 numerical aperture oil immersion objective (Leica Microsystems) under the same conditions used for the solutions. Image size was set to 512×512 pixels and scan speed was adjusted depending on fluorescence intensity (usually 400 Hz). The pinhole aperture was set to 1.46 Airy (163.26 μm confocal aperture). Additional measurements were taken using polarized light at 0° and 90°. In case of measurements on solid BBS, crystals were grown from BBS solutions in 1,2-dichlorobenzene by slow evaporation in solvent-saturated atmosphere of solution drops on microscope glass slides or glass coverslips. Crystals were then imaged using a 20.0× 0.5 numerical aperture dry objective (Leica Microsystems), a laser repetition rate of 20 MHz, an image size of 512×512 pixels and a scan speed adjusted depending on fluorescence intensity (usually 200 Hz). The pinhole aperture was set to 1.52 Airy (169.79 μm confocal aperture). Additional measurements were taken using polarized light at 0° and 90°. Two collection ranges were adopted for films imaging, from 440 to 480 nm (monomeric BBS) and from 530 to 620 nm (aggregated BBS), respectively, by using the built-in acousto-optical beam splitter (AOBS) detection system of the confocal microscope. Time-resolved emission spec-

tra (TRES) were recorded in the 420-700 nm range with 5 nm detection band width and 4 nm lambda detection stepsize. Imaging data were analysed using PicoQuant SymphoTime and FluoFit softwares.

1.3 Computational details

All the DFT and TD-DFT calculations were performed by using the M06-2X functional,[25] which has been shown to give accurate geometries and energies for a variety of systems dominated by dispersion interactions, such as DNA and benzene aggregates and represents a promising tool for the calculation of structural and spectroscopic properties of different types of non-covalent complexes.[26] Bulk solvent effects were included by using the Polarizable Continuum Model (PCM).[27,28] Such an approach has the advantage of lower computational cost with respect to an all-atoms approach where the solute-solvent interaction are taken into account explicitly.[29,30] It gives however a reasonably good description for solute-solvent interactions for systems dominated by electrostatic effects.[31–33]

The geometry of the BBS crystal was extracted from the experimental structure.[20] Starting from the crystal geometry we firstly focus on the two monomeric experimental conformers, which differ by the relative position of the N and O atoms. The geometry of the BBS monomers was then optimized by using the 6-31+G* basis set. It is important to stress that two of the six solvents discussed in the experimental section, 1,2-dichlorobenzene and ethyl butanoate, do not posses a PCM model and therefore were not taken into account for this reason. The calculation of vibronic spectra was performed by exploiting the Adiabatic Shift (AS) and Adiabatic Hessian (AH) approaches.[34–37] While AS only takes into account displacements of initial and final state minima, AH introduces Duschinsky effects through the computation of the Hessian matrices of both the initial and final states, including normal mode rotations upon the electronic transition.[38] AH and AS calculations were performed with the 6-31+G* basis set.

The starting point to define aggregates' structures was also in this case the experimental crystal structure.[20] From such a structure three kinds of aggregates were extracted and considered in the computational segment of this study: slide (**SL**), herringbone (**HB**) and stacked (**ST**), see Figure 1. All calculations were performed by using GAUSSIAN 16.[39]

2 Results and discussion

2.1 BBS dilute solutions

2.1.1 Absorption and emission spectra

BBS shows an absorption maximum centered around 370 nm and poorly dependent on the solvent properties (Figure 2(a) and Table 1), as revealed by absorption spectra of diluted (10^{-5} M) solutions. Molar extinction coefficients ε reported in Table 1 were calculated both in PrCOOEt and AcOEt as the slope of the line fitting the values of the absorption maximum *vs* concentration, obtaining 86718 and 79187 $l{\cdot}mol^{-1}{\cdot}cm^{-1}$ respectively (see Figure S1 in ESI). Fluorescence spectra obtained by exciting diluted solutions of BBS in different solvents at 360 nm (Figure 2(b)) show a vibronic structure composed by two major peaks around

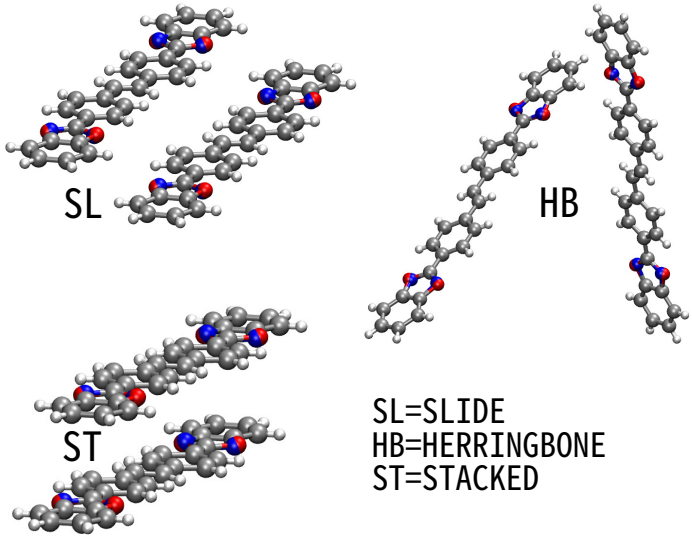

Figure 1 Definition of slide, herringbone and stacked aggregates for all the possible conformers. (The reference conformers are reported in Figure 3).

405 and 425 nm and a minor peak around 455 nm attributed to the 0-0, 0-1 and 0-2 radiative transitions respectively, with a very small shift in the emission maxima depending on the solvent (see Table 1). Fluorescence quantum yield ϕ_f of BBS was calculated as described in the methods; results showed a quantum yield of 0.79 in PrOH, 0.77 in AcOEt and 0.78 in CH_2Cl_2, as reported in Table 1, in good agreement with the values reported for similar compounds by Reiser *et al.*[40] The polarized emission of BBS was also investigated in terms of fluorescence anisotropy. When the transition moments of absorption and emission lie along specific axes of the fluorophore structure,molecules having their absorption transition moments oriented along the electric vector of the polarized incident light are preferentially excited, making the excited-state population partly oriented. Emission can be totally or partially depolarized due to several processes including fluorophore rotational diffusion, which is influenced by solvent viscosity and by the size and shape of the rotating fluorescent molecule.[41] The residual polarization of BBS can be described in terms of fluorescence anisotropy r calculated according to Equation 1, where $I_{\parallel}$ and $I_{\perp}$ are the parallel and perpendicular emission intensities with respect to the excitation plane. As expected, higher solvent viscosity induces higher anisotropy.

$$r = \frac{(I_{\parallel} - I_{\perp})}{(I_{\parallel} + 2I_{\perp})} \quad (1)$$

As reported in a previous work by some of the present authors,[15] BBS has two energy minima conformations referred here as M1 and M2 and depicted in Figure 3. M1 and M2 are almost isoenergetic (the absolute value of the energy difference in gas phase, computed at the M06-2X/6-31+G* level, is ΔE_{M1-M2} = 1.457075 kcal/mol), so that it is reasonable to assume the solution to be composed of M1 and M2 in comparable amounts. We performed a scan around two bonds, B1/B3

Table 1 Experimental absorption wavelength maxima (λ_{abs}), molar extinction coefficients (ε), emission wavelength maxima (λ_{em}), fluorescence quantum yield (ϕ_f) and anisotropy (r) of BBS in different solvents. [(a)] Fluorescence standard: quinine sulphate, ϕ_{QS} = 0.54. [(b)] Solvent viscosity (cP, 20 °C) is reported in brackets.

Solvent	λ_{abs} (nm)	ε (l·mol^{-1}·cm^{-1})	λ_{em} (nm)	$\phi_f^{(a)}$	$r^{(b)}$
2-Propanol	370	—	404, 428, 452	0.79	0.15 (2.40)
Ethyl acetate	369	79187±927	402, 423, 453	0.77	0.05 (0.45)
Ethyl butanoate	370	86718±251	401, 424, 453	—	—
Dichloromethane	373	—	406, 430, 457	0.78	0.05 (0.44)
Toluene	374	—	408, 432, 459	—	—

(see Figure 3), to observe the energy barrier (ΔE) needed for the conformers transition. The ΔE was computed both in vacuum and in AcOEt at the M06-2X/6-31+G* level of theory and results to be ΔE_{Vacuum}=0.3087eV (7.118789kcal/mol), ΔE_{AcOEt}=0.2718eV (6.267855kcal/mol) and ΔE_{Vacuum}=0.1859eV (4.286955kcal/mol), ΔE_{AcOEt}=0.2006eV (4.625945kcal/mol) around B1 and B3 respectively (see Figure S3 in ESI). The energy barrier around B3 results to be lower with respect to the one of B1, but anyhow an order of magnitude higher than K_BT=0.0257eV (0.5926559kcal/mol). The same results were observed for the vertical excitation transition.

A reliable calculation of absorption ($S_0 \rightarrow S_1$) and fluorescence ($S_0 \leftarrow S_1$) spectra first require a careful optimization of the ground and first singlet excited states geometries. Moving from the ground (S_0/GS) to the excited state (S_1) of M1, a remarkable change can be observed in the intramolecular geometrical parameters, particularly in the bonds lengths. The largest difference between the GS and S_1 is found for the B3, B4 and B5 distances. This corresponds to an increase in the quinoidal character of the orbitals in the six atom rings following the electronic transition, which has a HOMO → LUMO character. The distances most affected by the excitation process are those labeled in Figure 3; their percentages of variation are reported in Table S1 in the ESI. Similar values are obtained for the M2 conformer.

Calculated vibrationally resolved absorption/emission (ABS/EMI) spectra and vertical excitation/deexcitation (VE/VD) values for M1 and M2 do not show significant differences (see Figure S2 given in the ESI). Therefore, the following discussion will only focus on M1. Computed ABS/EMI spectra of BBS (M1) in AcOEt and Toluene are reported in Figure 4 (the same spectra in CH_2Cl_2 and PrOH can be found in Figure S4 of the ESI). Spectra obtained by simply considering VE/VD values (violet and blue lines) are compared with those calculated by considering electron-nuclei coupling (solid black lines), within the AS approach. Computed data are also compared with their experimental counterparts (dotted black line). The violet and blue curves in Figure 4 differ in the way solvent nonequilibrium effects are modelled, i.e. on whether a linear response approach (violet) or a solvent state specific (SS) response approach (blue)

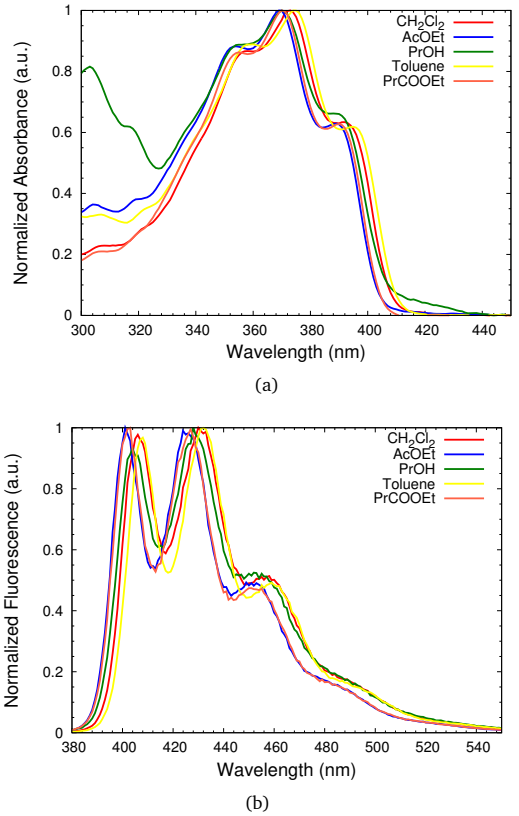

Figure 2 Experimental absorption (a) and fluorescence (b) spectra obtained from diluted solutions of BBS in different solvents (λ_{ex} for fluorescence spectra: 360 nm).

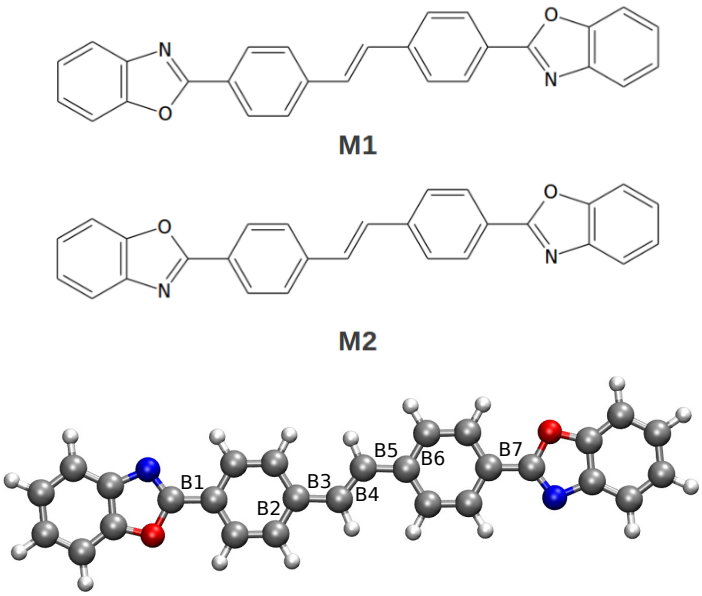

Figure 3 Molecular structure and atom labelling of the two BBS conformers M1 and M2.

is exploited.[42] In the case of VE/VD the resulting ABS/EMI bands consist of a single vertical transition, which is artificially broadened through convolution with a Gaussian function. The use of a more physically consistent state-specific approach to solvation shifts the absorption bands in all cases, however the description of the experimental spectrum is still poor. In fact, as it is clearly shown by Figure 4, the modeling of BBS spectra by only resorting to the calculation of vertical excitation/deexcitation energies is inadequate, because the experimental spectrum is dominated by vibronic effects. In fact, the consideration of vibronic effects in calculated spectra increases the quality of the description of the experiments. Remarkably, calculated spectra in 2-propanol are those worst matching experimental values (see Figure S4(b) in ESI). These findings are not surprising, because the purely continuum approach we have exploited to model solvent effects can reasonably be inadequate to treat specific hydrogen-bonding like interactions occurring between BBS and this solvent. In order to get more insight into the role

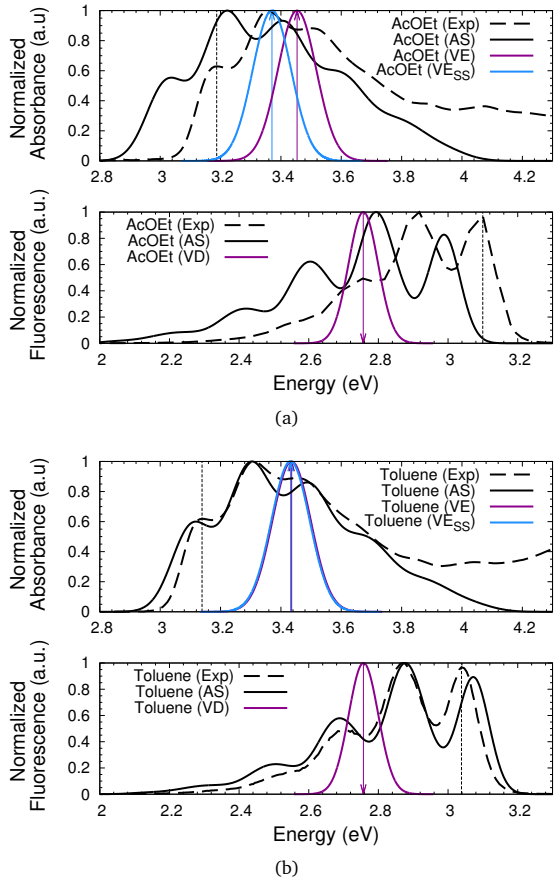

Figure 4 Calculated BBS absorption and emission spectra in various solvents obtained through vertical excitation (violet: solvent linear response, blue: state specific solvation) and the AS approach. All calculated spectra were obtained by summing oscillator strengths weighted Gaussian curves with a Full Width at Half Maximum (FWHM) of 0.15 and 0.1eV for the absorption and emission case respectively. Experimental spectra of diluted (10^{-5} M) solutions are also reported to comparison's sake.

of vibronic effects, and on the way they are computationally evaluated, in Figure 5 and 6 calculated absorption and emission spectra in toluene and AcOEt are more closely compared with their experimental counterparts (the same spectra in CH_2Cl_2 and PrOH can be found in Figure S5 and S6 of the ESI). Computed spectra were shifted along the energy axis to best match the position of the 0-0 vibronic transition of the experimental band. Shifts used are listed in Table 2 for the four solvent considered in this work. Clearly, shifts increase as increasing the solvent polarity and moving from the AS to the AH approach, which differ in the way differences in the normal modes between the ground and the excited state are considered (see[35,43] for more details). For both methods, the general shape as well as the relative band spacing of the computed spectra are very similar, showing that Duschinsky effects[44] are small for this system. Also, calculated spectra are in excellent agreement with the experiments, thus showing the reliability of our computational approach to describe the photophysics of BBS in the selected solvents.

2.1.2 TRES and FLIM analysis

The evolution of the emission spectrum with time was followed by recording time-resolved emission spectra (TRES) of BBS solutions in different solvents (λ_{ex} = 405 nm). Two organic esters, AcOEt and PrCOOEt, were chosen as reference solvents (in spite of their low solubilization power towards BBS) because of their chemical affinity with the polymers used as matrices for BBS dispersion in the forthcoming experiments. For concentrations of about 10^{-5} M, fluorescence spectra showed the expected peaks at 425 and 455 nm in both the chosen solvents. No relevant aggregation phenomena were detected, and a single fluorescence lifetime τ of 0.85 ns (monomeric BBS) was measured by FLIM. As expected, this lifetime value is shorter than that of unsubstituted stilbene (1.6 ns), since the benzoxazolyl substituents enhance the fluorescence efficiency. In stilbene-like molecules, this happens because the benzoxazolyl groups induce decrease of the rates of non-radiative processes such as *trans-cis* isomerization, which for this family of molecules is the main opponent of radiative decay.[40] The time-resolved spectra (Figure S7 in ESI) show only minor changes with time (up to 20 ns), since excimer formation is prevented by the short lifetime and fast diffusion rate of the monomer.[16]

2.2 BBS aggregates

In time-resolved experiments on more concentrated solutions (10^{-4} M) the presence of an excimer is revealed by the rising of a broad peak around 540 nm, followed by the disappearance of the two main peaks under 460 nm on a time scale of about 10 ns as shown in Figure 7(a) and 7(b). FLIM analysis revealed an additional decay lifetime greater than 3 ns that we shall tentatively ascribe to the excimeric complex, more clearly visible in AcOEt, which is a worse solvent for BBS. The excimer formation is possible thanks to the π stacking of different BBS molecules with associated excited electronic states. Evaluation of the diffusion process of BBS in solution (see Equations 2-4), calculated using the value 0.8×10^{-9} $m^2{\cdot}s^{-1}$ for the diffusion coefficient D as obtained from NMR data by Fourati *et al.*[45], showed that the probability (P_0) of two independent molecules being in the col-

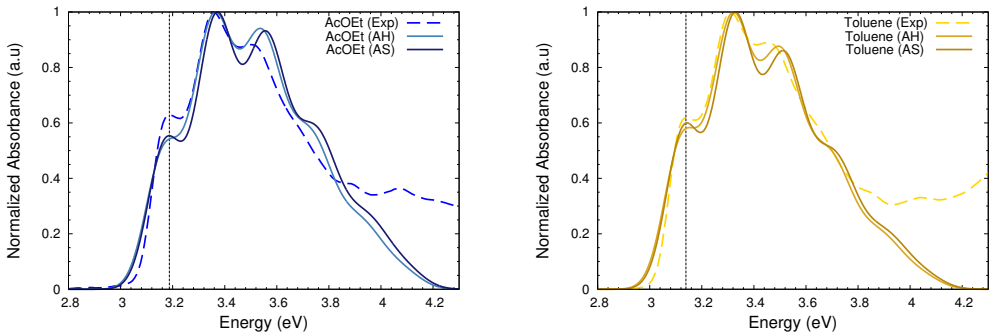

(a) (b)

Figure 5 Calculated vibrationally resolved absorption spectra of M1 in different solvents using the AH and AS approach are compared with the experimental spectra of diluted (10^{-5} M) solutions. All calculated spectra were obtained by summing normalized molar absorption coefficient weighted Gaussian curves with a Full Width at Half Maximum (FWHM) of 0.15 eV for each calculated energy value.

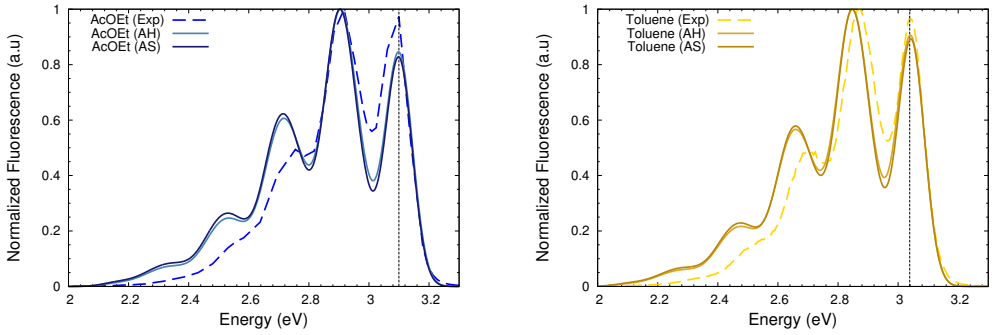

(a) (b)

Figure 6 Calculated vibrationally resolved emission spectra of M1 in different solvents using the AH and AS methods are compared with the experimental spectra of diluted (10^{-5} M) solutions. All calculated spectra were obtained by summing normalized energy emitted by one mole per second weighted Gaussian curves with a Full Width at Half Maximum (FWHM) of 0.1 eV for each calculated energy value.

Table 2 Energy shifts used to match the position of the 0-0 vibronic transition to the experimental band for absorption and emission spectra. Values for both AH and AS approaches are reported. The dielectric constant ε and square of refractive index n^2 are also reported for the four solvent here considered.

Solvent	ε	n^2	AH_{Abs} (eV)	AS_{Abs} (eV)	AH_{Emi} (eV)	AS_{Emi} (eV)
Toluene	2.3741	2.238	0.085	0.025	0.045	-0.030
Ethyl acetate	5.9867	1.882	0.21	0.15	0.187	0.110
Dichloromethane	8.9300	2.028	0.21	0.15	0.169	0.093
2-Propanol	19.264	1.900	0.30	0.22	0.183	0.103

lision volume (V) in the range of concentration used (C) and on a 10 ns time scale (τ) is less than 0.1%, thus making a collision highly unlikely to happen.

$$P_0 = 1 - e^{-VNC} \tag{2}$$

$$V = \frac{4}{3}\pi w^3 \tag{3}$$

$$w^2 = 4D\tau \tag{4}$$

Therefore, it sounds convincing that a pre-coordinated dimeric form must already exist at the fundamental state to allow the formation of the detected excimer. The occurrence of this pre-coordination is promoted by higher concentrations of fluorophore in the solution and, likely, this effect is less significant in PrCOOEt due to a higher solvation efficiency towards BBS that leads to disruption of the pre-coordinated couples. To investigate the behavior of BBS in a diametrically opposed situation, isolated crystals of BBS were prepared by slow evaporation of its solutions. In this case, the molecules are organized in a compact structure, corresponding to a very high aggregation state, and oriented in space as confirmed by the high anisotropy features revealed by confocal fluorescence microscopy upon irradiation with polarized light (see Figure S8 in ESI). The steady-state emission spectrum showed the expected band around 510 nm (Figure 8(a) red curve), attributed to aggregated BBS molecules, while TRES measurements revealed the presence of excimers with the raising of the band around 540 nm after a few nanoseconds (Figure 9(a)).

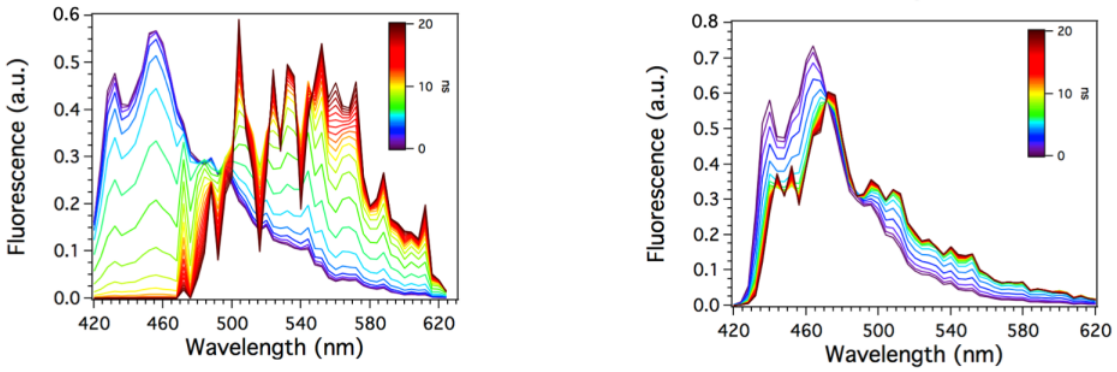

(a) (b)

Figure 7 Time-resolved emission spectra of BBS 10^{-4} M in (a) AcOEt and (b) PrCOOEt.

FLIM analysis of the crystals gave four different lifetimes of 0.5, 1.8, 3.8, and 9.3 ns, associated with four different available microstates for the molecules in the crystal structure.

As reported by Fourati *et al.*,[20] the structure of BBS aggregates features a network composed of layers in the *bc* plane with molecules packed in a well-defined herringbone pattern. Within the layers, the flat molecules are packed via π-π stacking interactions and C-H$\cdots\pi$ contacts (see Figure 1). The π-π stacking interactions feature a short centroid-centroid distance between the central and the terminal benzene rings. The π-stacked molecules are staggered relative to one another and the benzene rings overlap at a well-defined distance. Moreover, a C-H$\cdots\pi$ contact involves an interaction between the terminal hydrogen atom and the terminal benzene ring centroid of two molecules.

In order to get more insight into the structure of the aggregates and their photophysical properties, various kind of dimers were extracted from the crystal structure, labeled by a symbol: **ST** (stacked), **SL** (slide) and **HB** herringbone with reference to their relative orientation, and by a number: **1** (M1-M1), **2** (M1-M2) or **3** (M2-M2), related to the combination of the monomers composing them.

Excitation energies of the dimers were then calculated at the M06-2X/6-31+G* level in two alternative situations: AcOEt and a non-polar environment, with dielectric constant $\varepsilon = 2.5$, and refraction index $n = 1.5$ (ε_∞=n^2=2.25), mimicking a polymeric matrix (such as the cyclic olefin copolymer (COC) experimentally used in[17] see also Fig.S9 in the ESI). Notice that the structures extracted from the crystal structure were not further optimized. Vertical excitational energies for the first three singlet excited states are reported in Table 3 and Table S2 for COC and AcOEt, respectively. As expected, dimers excitation energies differ from those of the monomers, that due to the coupling between the excited-states of the monomers. In particular, excitation energies increase in both the analyzed environments moving from the monomers to the **ST** dimers and then to the **SL** dimers (e.g. $E_{M1_{S1}}$=3.6440 eV < $E_{ST1_{S2}}$=3.6626 eV < $E_{SL1_{S2}}$=3.6779 eV). Different from the other cases, for the **HB** configuration, two transitions are indeed populated, showing respectively lower and higher excitation energies with respect to monomers (e.g. $E_{HB1_{S1}}$=3.6260 eV < $E_{M1_{S1}}$=3.6440 eV < $E_{HB1_{S2}}$=3.6633 eV). This behavior can be ascribed to the **HB** geometry: the mean distance between the monomers is indeed increased with respect to the **ST** and **SL** dimers, however the excimer formation still seems to occur. These observations are in accordance with experimental data: the aggregation process indeed leads to a shift of absorption peaks to shorter wavelengths, as it is reported in Figure S9.

Table 3 M06-2X/6-31+G* COC ($\varepsilon = 2.50$, ε_∞=2.25) vertical excitation energies (in eV) and oscillator strengths (f) of M1, M2 and of different dimer structures (ST:Stacked, SL:Slide, HB:Herringbone) extracted from the crystal structure[20].

	States			
	S1	**S2**	**S3**	**Orientation**
E	*3.6440*	*4.5093*	*4.8008*	*M1*
f	*2.6027*	*0.0000*	*0.0256*	
E	*3.6432*	*4.5148*	*4.8059*	*M2*
f	*2.5810*	*0.0011*	*0.0290*	
E	*3.4975*	*3.6626*	*4.1797*	*ST1*
f	*0.0000*	*5.0020*	*0.0401*	
E	*3.4889*	*3.6629*	*4.1670*	*ST2*
f	*0.0010*	*4.9710*	*0.0400*	
E	*3.4911*	*3.6636*	*4.1765*	*ST3*
f	*0.0001*	*4.9598*	*0.0216*	
E	*3.6067*	*3.6779*	*4.4783*	*SL1*
f	*0.0011*	*5.0988*	*0.0010*	
E	*3.6073*	*3.6758*	*4.4798*	*SL2*
f	*0.0013*	*5.0756*	*0.0022*	
E	*3.6048*	*3.6763*	*4.4765*	*SL3*
f	*0.0011*	*5.0508*	*0.0007*	
E	*3.6260*	*3.6633*	*4.4933*	*HB1*
f	*2.0215*	*3.2080*	*0.0009*	
E	*3.6260*	*3.6626*	*4.4952*	*HB2*
f	*2.0209*	*3.1864*	*0.0008*	
E	*3.6255*	*3.6621*	*4.4991*	*HB3*
f	*2.0245*	*3.1597*	*0.0025*	

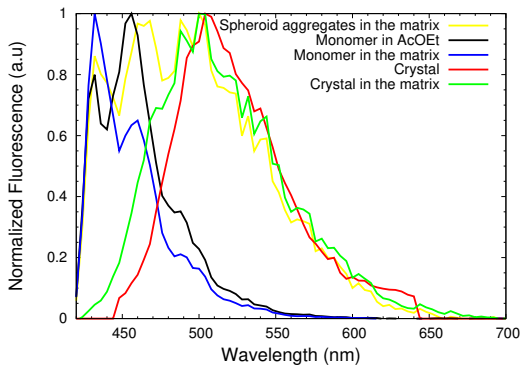

Figure 8 (a) Steady-state fluorescence spectra of BBS: spheroid aggregates in PLA (yellow, BBS concentration of 0.1 w/w); 10^{-5} M in AcOEt (black); homogeneously dispersed monomer in PLA (blue, BBS concentration of 0.05 w/w); anisotropic crystals in PLA (green, BBS concentration of 0.2 w/w); isolated BBS crystals (red). (b) Steady-state fluorescence spectra of BBS in the isolated crystal and decay-associated spectra of four different microstates.

Additionally, decay-associated spectra (DAS) of the crystals were calculated. A DAS is a spectrum that represents the emission of a state with a particular decay lifetime. Given the global steady-state emission spectrum at a fixed wavelength, and the relative percentage of that intensity belonging to each decay component from the lifetime measurements, plotting each component as a fraction of the total intensity gives the emission spectrum of the relevant microstate. According to Equation 5, $DAS_i(\lambda)$ corresponds to the intensity of the ith component at a specific wavelength λ, $F_{ss}(\lambda)$ is the total intensity of the steady-state fluorescence of the crystal, $\alpha_i(\lambda)$ is the wavelength dependent amplitude and τ_i is the lifetime of the ith component.

$$DAS_i(\lambda) = F_{ss}(\lambda)\frac{\alpha_i(\lambda)\tau_i}{\sum_i \alpha_i(\lambda)\tau_i} \quad (5)$$

DAS spectra of BBS crystals (Figure 8(b)) revealed the position of the emission maxima of the four different microstates; it is worth stating that the longer the lifetime, the higher the emission wavelength. Notably, the main contribution to the global fluorescence is given by the two species with intermediate lifetimes. The position of the peak relevant to the longer lifetime induces the attribution of this component to excimers, thus suggesting the existence of a microstate compatible with excimer formation in the crystal.

2.3 BBS aggregates in a poly(L-lactic acid) (PLA) matrix

Aimed at investigating the aggregachromic behavior of BBS in polymeric materials, BBS/PLA blends were realized. PLA was selected as a dispersing medium due to its compatibility with BBS and because it had been previously investigated by the authors as a supporting polymer matrix in the preparation of smart materials.[18] When BBS was dispersed in the PLA matrix, a set of different situations was observed. At low BBS concentration (0.05 % w/w), most of the dye was homogeneously dispersed as a monomer within the matrix, even if small aggregates of spheroid shape can appear at that content as shown in Figure 10(a), where the fluorescent matrix is pseudo-coloured in blue (homogeneously dispersed monomers) and the spheroid aggregates in green.

Steady-state emission spectra taken from aggregate-free areas are similar to the spectrum of monomeric BBS in solution, except for the inversion of the relative heights of the two main vibrational bands (Figure 8(a), black and blue curves). FLIM analysis revealed a single lifetime of 0.8 ns, as for the dissolved monomeric dye, and no excimer formation was detectable from the TRES (Figure 9(b)). The size and shape of the micrometric aggregates that form in the matrix depend on the amount of fluorophore used for the blend. At low concentration (0.05 % w/w) small spheroid aggregates of about 800-900 nm in diameter start to assemble and are still present at a concentration of 0.1 % w/w, where some star-shaped crystals of about 10 μm in diameter also appear (Figure 10(b)). The spheroid aggregates give fluorescence spectra where the band of the monomer is still visible, but additionally a broad unstructured band due to the presence of aggregates appears around 500 nm (Figure 8(a), yellow curve). In about 6 ns the excimer emission band arises around 540 nm, as revealed by the time-resolved spectrum in Figure 9(c). At higher concentrations (0.2% w/w in the polymer matrix, Figure 10(c)) BBS starts forming crystals of peculiar helicoidal shape, with a diameter of about 2 μm and variable length, from a few tens to several hundreds of μm. Emission spectra of such crystals in the matrix are similar to those of isolated BBS crystals; peaks relevant to the monomeric form are not present, while the aggregate band is visible at 500 nm (Figure 8(a), green curve). Time-resolved experiments show the formation of the excimer band around 540 nm (Figure 9(d)), thus confirming that in their aggregate form (small aggregates or crystals) BBS molecules can easily coordinate to form excimeric complexes.

3 Conclusions

BBS solutions and dispersions in a PLA matrix at different concentration were investigated in detail by an effective combination of high-resolution optical imaging techniques and quantum-mechanical calculations. At low BBS content, the investigations revealed the presence of isolated BBS monomers in solution as well as in PLA dispersions, even if in the latter case nano- and micro-sized BBS supramolecular spheroids start to appear with

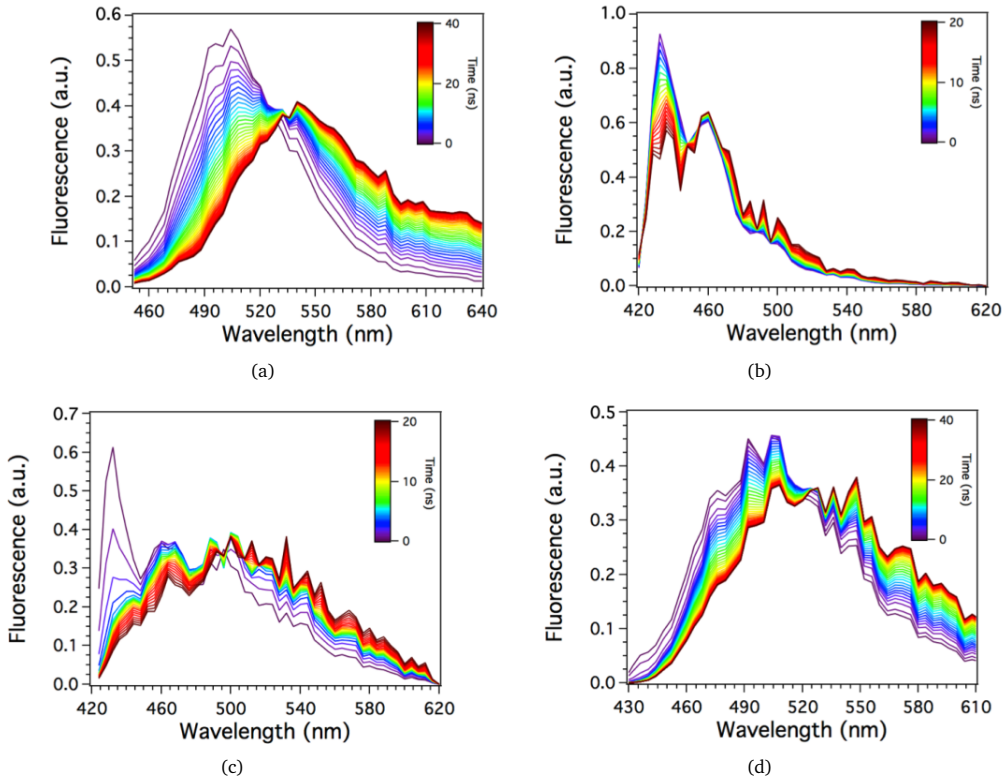

Figure 9 Time-resolved emission spectra of isolated pure BBS crystals (a), homogeneously dispersed BBS monomer in PLA (b), spheroid BBS aggregates in PLA (c) and BBS crystals in PLA (d).

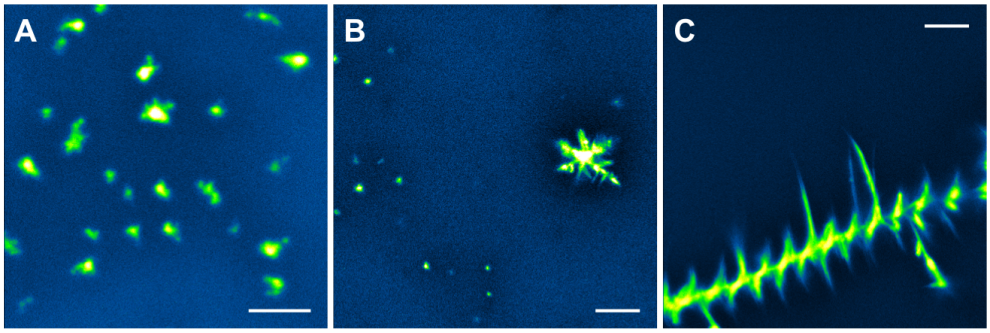

Figure 10 Pseudo-colour confocal images in the 530-620 nm range of BBS 0.05% (A), 0.1% (B) and 0.2% (C) w/w in PLA. Scale bars: 5 μm.

increasing fluorophore content. Above a certain concentration threshold (10^{-4} M in solution and 0.1% w/w in PLA) the typical BBS emission attributed to the formation of excimers appeared, caused by the assembly of BBS molecules in different geometries, similar to what already reported experimentally.[20] The formation of excimers in solution resulted subjected to the presence of a pre-coordinated dimeric form at the fundamental state. Notably, the polymer matrix was able to modulate the geometry of BBS aggregates that changed from spheroids to anisotropic microsized helices depending on the fluorophore concentration. Overall, the combination of experimental and theoretical investigations proposed in this work provides effective and informative methodologies able to correlate the optical features of BBS with the preferential geometry of its assemblies depending on the dispersing media and concentration. Moreover, the approach appears very suitable for modulating the optical response of BBS-doped polymer blends, providing useful information for the development of smart materials and devices.

4 Acknowledgements

We are thankful for the computer resources provided by the high performance computing facilities of the SMART Laboratory (http://smart.sns.it/). CC gratefully acknowledges the support of H2020-MSCA-ITN-2017 European Training Network "Computational Spectroscopy In Natural sciences and Engineering" (COSINE), grant number 765739.

References

1 C. M. Lampert, *Materials today*, 2004, **7**, 28–35.
2 A. Pucci, R. Bizzarri and G. Ruggeri, *Soft Matter*, 2011, **7**,

3689–3700.
3 S. A. Jenekhe and D. J. Kiserow, *D. J. Kiserow*, ACS Publications, 2004.
4 M. W. Urban, *Handbook of stimuli-responsive materials*, John Wiley & Sons, 2011.
5 A. Pucci and G. Ruggeri, *J. Mater. Chem.*, 2011, **21**, 8282–8291.
6 F. Donati, A. Pucci, C. Cappelli, B. Mennucci and G. Ruggeri, *J. Phys. Chem. B*, 2008, **112**, 3668–3679.
7 K. M. Herbert, S. Schrettl, S. J. Rowan and C. Weder, *Macromolecules*, 2017, **50**, 8845–8870.
8 J. Mei, N. L. Leung, R. T. Kwok, J. W. Lam and B. Z. Tang, *Chem. Rev.*, 2015, **115**, 11718–11940.
9 P. Minei and A. Pucci, *Polym. Int.*, 2016, **65**, 609–620.
10 M. Carlotti, E. Fanizza, A. Panniello and A. Pucci, *Solar Energy*, 2015, **119**, 452–460.
11 C. Haines, M. Chen and K. P. Ghiggino, *Solar Energy Materials and Solar Cells*, 2012, **105**, 287–292.
12 I. M. Ward, *Structure and properties of oriented polymers*, Springer Science & Business Media, 2012.
13 A. J. Bur and S. C. Roth, *Polym. Eng. Sci.*, 2004, **44**, 898–908.
14 A. Pucci, M. Bertoldo and S. Bronco, *Macromol. Rapid Commun.*, 2005, **26**, 1043–1048.
15 A. Pucci, C. Cappelli, S. Bronco and G. Ruggeri, *J. Phys. Chem. B*, 2006, **110**, 3127–3134.
16 A. Pucci, F. Di Cuia, F. Signori and G. Ruggeri, *J. Mater. Chem.*, 2007, **17**, 783–790.
17 F. Donati, A. Pucci, L. Boggioni, I. Tritto and G. Ruggeri, *Macromol. Chem. Phys*, 2009, **210**, 728–735.
18 A. Pucci, F. Signori, R. Bizzarri, S. Bronco, G. Ruggeri and F. Ciardelli, *J. Mater. Chem.*, 2010, **20**, 5843–5852.
19 C. E. Sing, J. Kunzelman and C. Weder, *J. Mater. Chem.*, 2009, **19**, 104–110.
20 M. A. Fourati, T. Maris, C. G. Bazuin and R. E. Prud'homme, *Acta Crystallogr., Sect. C: Cryst. Struct. Commun.*, 2010, **66**, o11–o14.
21 A. Battisti, P. Minei, A. Pucci and R. Bizzarri, *Chem. Commun.*, 2017, **53**, 248–251.
22 A. T. R. Williams, S. A. Winfield and J. N. Miller, *Analyst*, 1983, **108**, 1067–1071.
23 J. Shen and R. D. Snook, *Chem. Phys. Lett.*, 1989, **155**, 583–586.
24 W. Melhuish, *J. Phys. Chem.*, 1961, **65**, 229–235.
25 Y. Zhao and D. G. Truhlar, *Theor. Chem. Acc.: Theory, Computation, and Modeling (Theoretica Chimica Acta)*, 2008, **120**, 215–241.
26 Y. Zhao and D. G. Truhlar, *Acc. Chem. Res.*, 2008, **41**, 157–167.
27 M. Cossi, N. Rega, G. Scalmani and V. Barone, *J. Comput. Chem.*, 2003, **24**, 669–681.
28 A. Biancardi, R. Cammi, C. Cappelli, B. Mennucci and J. Tomasi, *Theor. Chem. Acc.*, 2012, **131**, 1157.
29 H. M. Senn and W. Thiel, *Angewandte Chemie International Edition*, 2009, **48**, 1198–1229.
30 A. Warshel and M. Levitt, *Journal of molecular biology*, 1976, **103**, 227–249.
31 F. Egidi, V. Barone, J. Bloino and C. Cappelli, *J. Chem. Theory Comput.*, 2012, **8**, 585–597.
32 F. Egidi, T. Giovannini, M. Piccardo, J. Bloino, C. Cappelli and V. Barone, *J. Chem. Theory Comput.*, 2014, **10**, 2456–2464.
33 B. Carlotti, A. Cesaretti, O. Cannelli, T. Giovannini, C. Cappelli, C. Bonaccorso, C. G. Fortuna, F. Elisei and A. Spalletti, *J. Phys. Chem. C*, 2018.
34 J. Bloino, A. Baiardi and M. Biczysko, *Int. J. Quantum Chem.*, 2016, **116**, 1543–1574.
35 M. Biczysko, J. Bloino, F. Santoro and V. Barone, *Computational Strategies for Spectroscopy*, 2012, 361–443.
36 O. Cannelli, T. Giovannini, A. Baiardi, B. Carlotti, F. Elisei and C. Cappelli, *PCCP*, 2017, **19**, 32544–32555.
37 J. Bloino, M. Biczysko, F. Santoro and V. Barone, *J. Chem. Theory Comput.*, 2010, **6**, 1256–1274.
38 A. Baiardi, J. Bloino and V. Barone, *J. Chem. Phys.*, 2016, **144**, 084114.
39 M. J. Frisch, G. W. Trucks, H. B. Schlegel, G. E. Scuseria, M. A. Robb, J. R. Cheeseman, G. Scalmani, V. Barone, G. A. Petersson, H. Nakatsuji, X. Li, M. Caricato, A. V. Marenich, J. Bloino, B. G. Janesko, R. Gomperts, B. Mennucci, H. P. Hratchian, J. V. Ortiz, A. F. Izmaylov, J. L. Sonnenberg, D. Williams-Young, F. Ding, F. Lipparini, F. Egidi, J. Goings, B. Peng, A. Petrone, T. Henderson, D. Ranasinghe, V. G. Zakrzewski, J. Gao, N. Rega, G. Zheng, W. Liang, M. Hada, M. Ehara, K. Toyota, R. Fukuda, J. Hasegawa, M. Ishida, T. Nakajima, Y. Honda, O. Kitao, H. Nakai, T. Vreven, K. Throssell, J. A. Montgomery, Jr., J. E. Peralta, F. Ogliaro, M. J. Bearpark, J. J. Heyd, E. N. Brothers, K. N. Kudin, V. N. Staroverov, T. A. Keith, R. Kobayashi, J. Normand, K. Raghavachari, A. P. Rendell, J. C. Burant, S. S. Iyengar, J. Tomasi, M. Cossi, J. M. Millam, M. Klene, C. Adamo, R. Cammi, J. W. Ochterski, R. L. Martin, K. Morokuma, O. Farkas, J. B. Foresman and D. J. Fox, *Gaussian 16 Revision B.01*, 2016, Gaussian Inc. Wallingford CT.
40 A. Reiser, L. Leyshon, D. Saunders, M. Mijovic, A. Bright and J. Bogie, *J. Am. Chem. Soc.*, 1972, **94**, 2414–2421.
41 B. Valeur and M. N. Berberan-Santos, *Molecular fluorescence: principles and applications*, John Wiley & Sons, 2012.
42 R. Improta, G. Scalmani, M. J. Frisch and V. Barone, *J. Chem. Phys.*, 2007, **127**, 074504.
43 M. Hodecker, M. Biczysko, A. Dreuw and V. Barone, *J. Chem. Theory Comput.*, 2016, **12**, 2820–2833.
44 F. Duschinsky, *Acta Physicochim. URSS*, 1937, **7**, 551–566.
45 M. A. Fourati, W. Skene, C. G. Bazuin and R. E. Prud'homme, *J. Phys. Chem. A*, 2013, **117**, 836–844.

Supporting Information

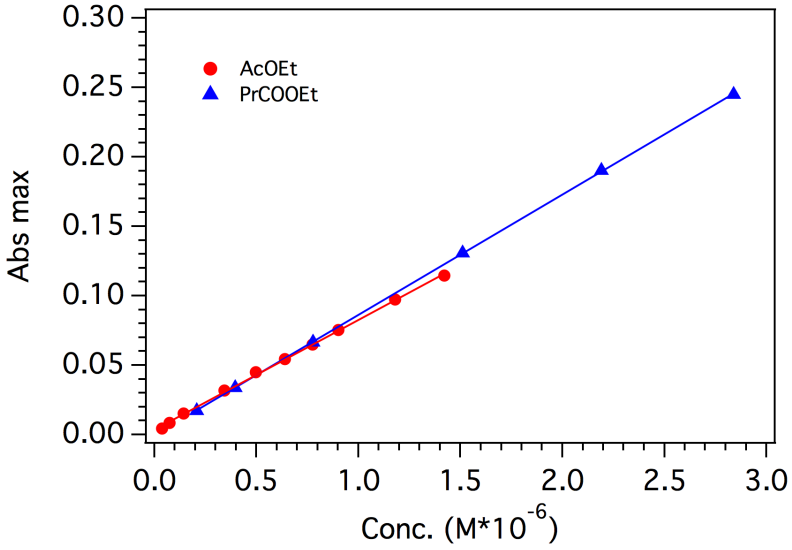

Figure S1 Absorbance maxima vs concentration for BBS solutions in AcOEt (red) and PrCOOEt (blue).

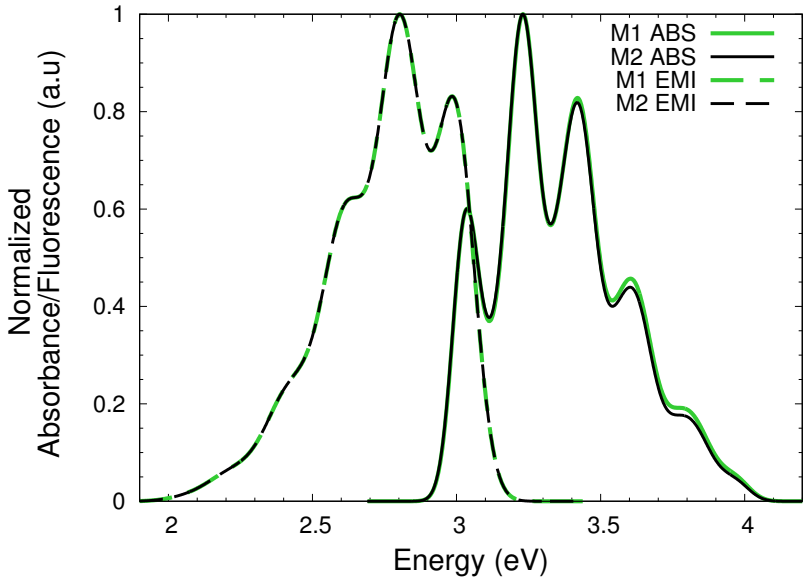

Figure S2 Calculated M06-2X/6-31+G* vibrationally resolved absorption and emission spectra of M1 and M2 in toluene, obtained by using the AH approach.

Geometrical Parameter	Percentage Change $S_0 \rightarrow S_1$
B1	-1.97%
B2	-2.17%
B3	-4.08%
B4	4.47%
B5	-4.08%
B6	-2.17%
B7	-1.97%

Table S1 BBS M1 structure. Calculated M06-2X/6-31+G* bond length variation resulting from the excitation process. Data are obtained in toluene solution.

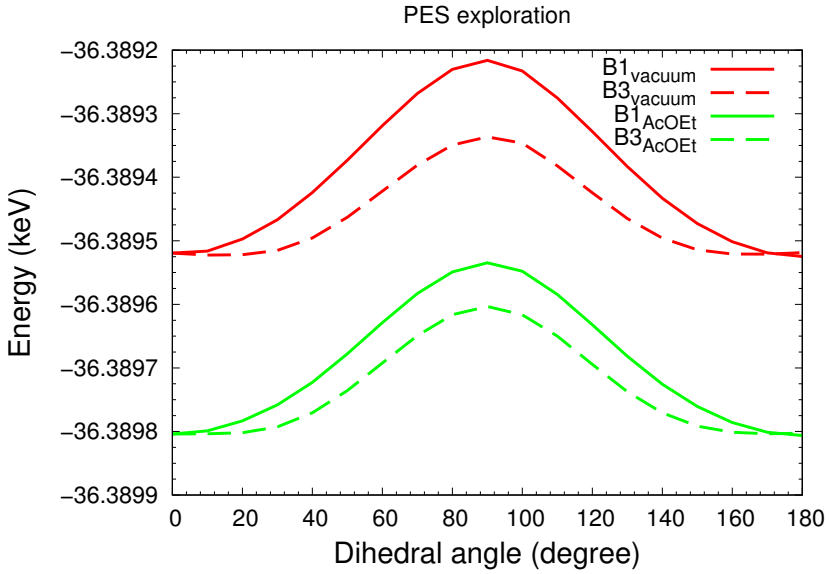

Figure S3 Scan around B1 and B3 bonds as reported in Figure 3 computed at M06-2X/6-31+G* level of theory in vacuum and in AcOEt.

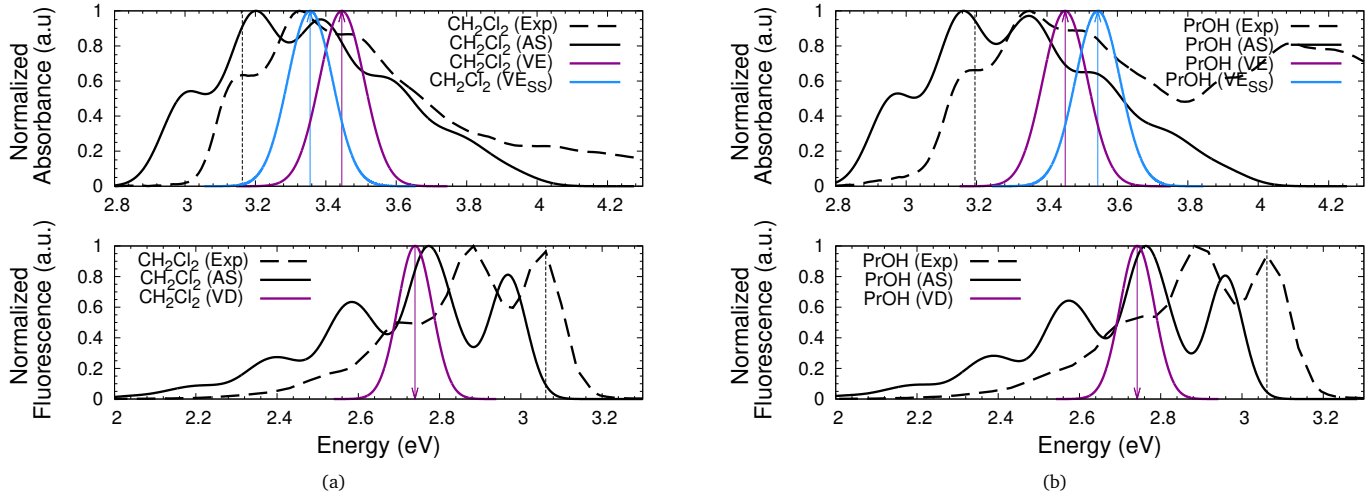

Figure S4 Calculated BBS absorption and emission spectra in various solvents obtained through vertical excitation (violet: solvent linear response, blue: state specific solvation) and the AS approach. All calculated spectra were obtained by summing oscillator strengths weighted Gaussian curves with a Full Width at Half Maximum (FWHM) of 0.15 and 0.1eV for the absorption and emission case respectively. Experimental spectra of diluted (10^{-5} M) solutions are also reported to comparison's sake.

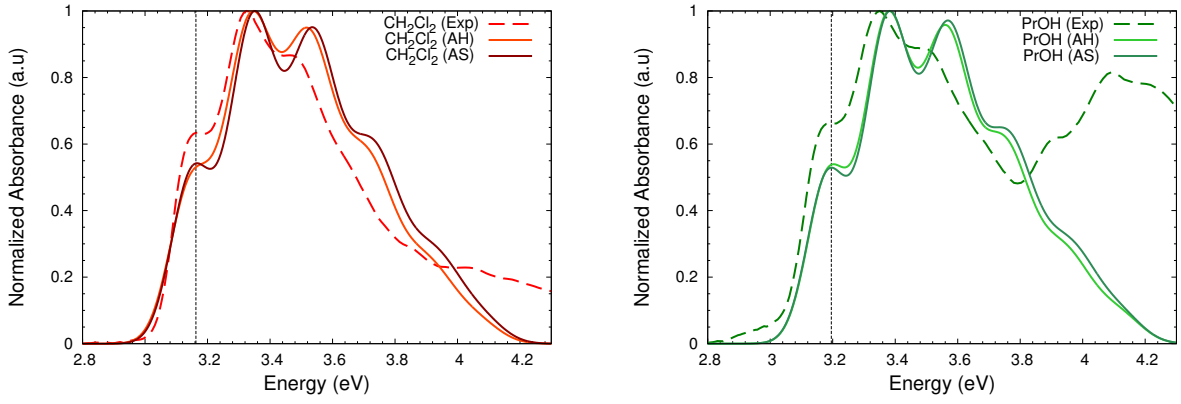

(a) (b)

Figure S5 Calculated vibrationally resolved absorption spectra of M1 in different solvents using the AH and AS approach are compared with the experimental spectra of diluted (10^{-5} M) solutions. All calculated spectra were obtained by summing normalized molar absorption coefficient weighted Gaussian curves with a Full Width at Half Maximum (FWHM) of 0.15 eV for each calculated energy value.

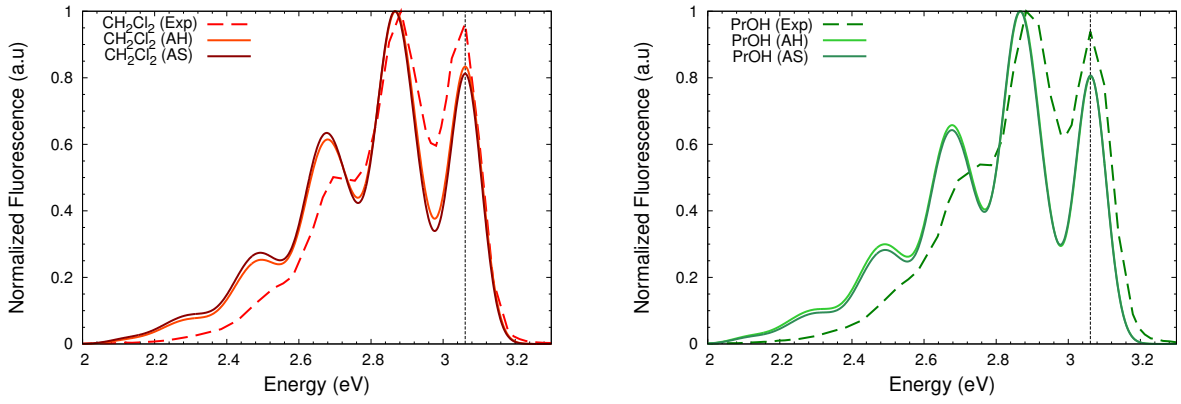

(a) (b)

Figure S6 Calculated vibrationally resolved emission spectra of M1 in different solvents using the AH and AS methods are compared with the experimental spectra of diluted (10^{-5} M) solutions. All calculated spectra were obtained by summing normalized energy emitted by one mole per second weighted Gaussian curves with a Full Width at Half Maximum (FWHM) of 0.1 eV for each calculated energy value.

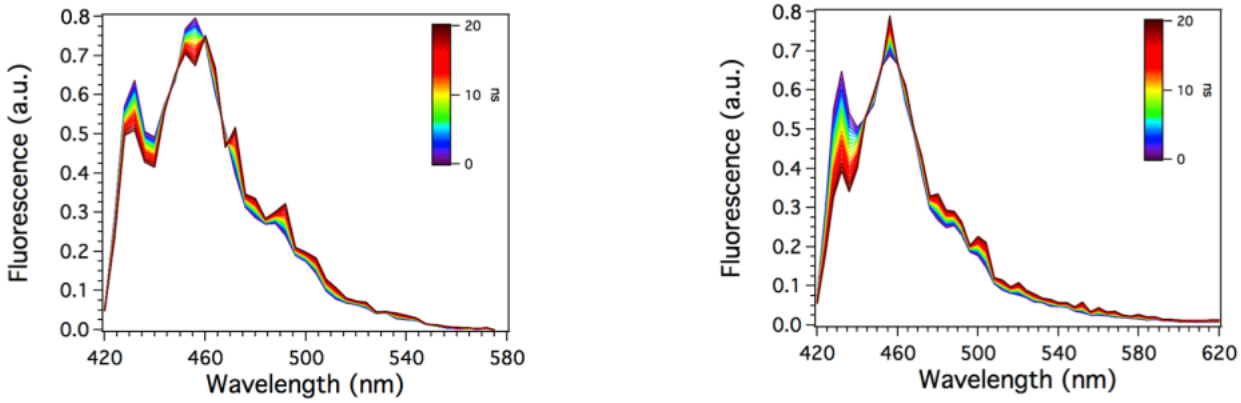

(a) (b)

Figure S7 Time-resolved emission spectra of BBS 10^{-5} M in (a) AcOEt and (b) PrCOOEt.

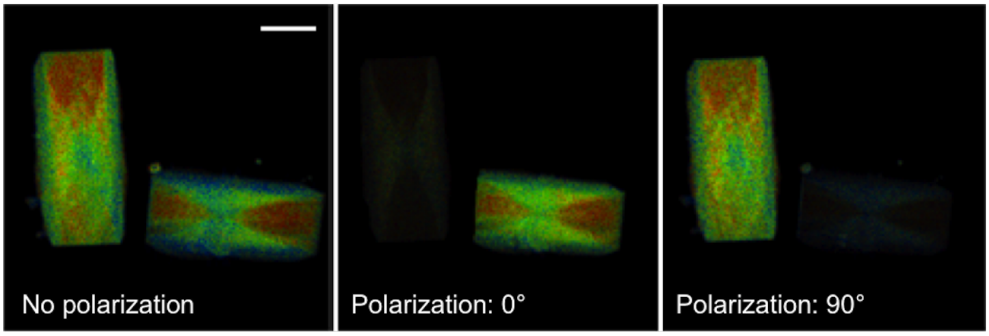

Figure S8 Pseudo-colour confocal images of BBS crystals fluorescence upon polarized light irradiation at 405 nm. Scale bar: 50 μm.

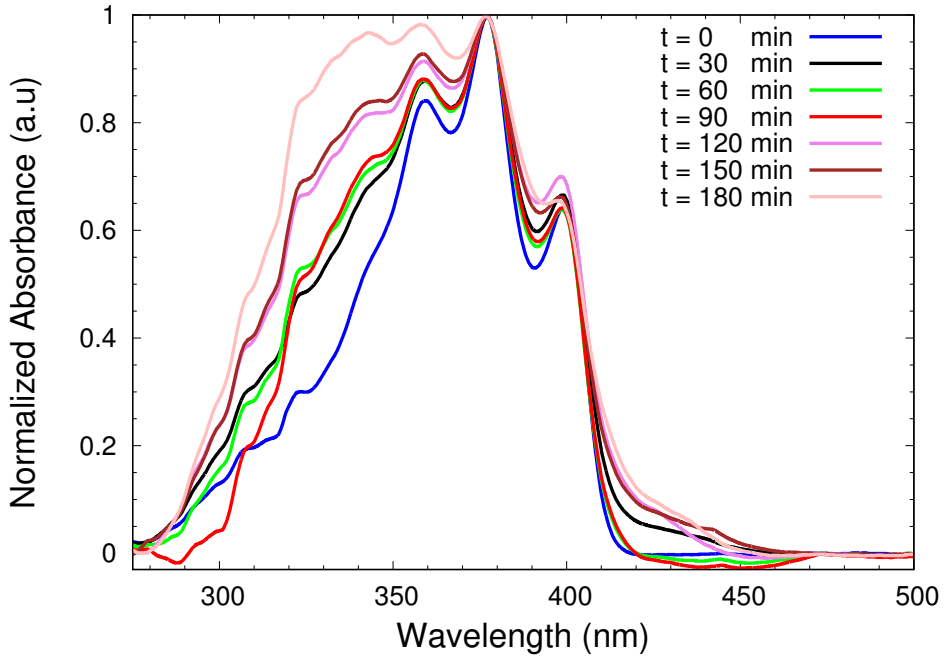

Figure S9 UV-Vis absorption spectra of a COC film containing the 0.5 wt.% of BBS during an annealing experiments aimed at favouring the formation of dye aggregates. The spectra are normalized to the absorption intensity attributed to the isolated BBS molecules at 377 nm.

Table S2 M06-2X/6-31+G* in AcOEt vertical excitation energies (in eV) and oscillator strengths (f) of M1, M2 and of different dimeric structures (ST:Stacked, SL:Slide, HB:Herringbone) extracted from the crystal structure[20] and not optimized.

	States			
	S1	**S2**	**S3**	**Orientation**
E	*3.5919*	*4.4314*	*4.7968*	*M1*
f	*2.6596*	*0.0000*	*0.0348*	
E	*3.5912*	*4.4383*	*4.8014*	*M2*
f	*2.6398*	*0.0017*	*0.0383*	
E	*3.4768*	*3.5984*	*4.1755*	*ST1*
f	*0.0000*	*5.2302*	*0.0332*	
E	*3.4687*	*3.5988*	*4.1639*	*ST2*
f	*0.0017*	*5.2021*	*0.0320*	
E	*3.4700*	*3.5992*	*4.1752*	*ST3*
f	*0.0002*	*5.1907*	*0.0199*	
E	*3.5757*	*3.6091*	*4.4172*	*SL1*
f	*0.0053*	*5.2718*	*0.0003*	
E	*3.5758*	*3.6076*	*4.4198*	*SL2*
f	*0.0067*	*5.2487*	*0.0014*	
E	*3.5743*	*3.6078*	*4.4196*	*SL3*
f	*0.0024*	*5.2328*	*0.0002*	
E	*3.5850*	*3.6028*	*4.4222*	*HB1*
f	*2.0329*	*3.3032*	*0.0004*	
E	*3.5848*	*3.6023*	*4.4236*	*HB2*
f	*2.0345*	*3.2812*	*0.0004*	
E	*3.5844*	*3.6019*	*4.4289*	*HB3*
f	*2.0417*	*3.2533*	*0.0018*	